mater.scichina.com link.springer.com

Published online 7 September 2020 | https://doi.org/10.1007/s40843-020-1440-6
Sci China Mater 2020, 63(12): 2606–2612

N-modulated Cu^+ for efficient electrochemical carbon monoxide reduction to acetate

Fenglou Ni[1], Hao Yang[2], Yunzhou Wen[1], Haipeng Bai[1], Longsheng Zhang[1], Chunyu Cui[1], Shangyu Li[1], Sisi He[1], Tao Cheng[2*], Bo Zhang[1*] and Huisheng Peng[1*]

The electrocatalytic approach of converting carbon dioxide (CO_2) to valuable chemical commodities and feedstocks provides a promising solution to store intermittent renewable electricity in a high-energy-density way and mitigate CO_2 accumulation in atmosphere [1–3]. Recently, the electrochemical CO_2 reduction reaction (CO_2RR) has made remarkable progress in yielding C_1 products (such as carbon monoxide (CO) [4–6] and formate ($HCOO^-$) [7–9]) with significantly high current densities and high Faradaic efficiencies (FEs). Meanwhile, the overall performance of CO_2RR to C_2 products of ethylene [10–12] and ethanol [13–15], has greatly improved on copper (Cu) catalysts. However, acetate (another C_2 product), which is wildly used as a raw chemical material for pharmacy, dyestuff, rubber and so on, has an excessively low partial current density (<1 mA cm^{-2}) and low FE (<20%) [16,17]. Kanan and coworkers [18] suggested that higher KOH concentrations may facilitate the formation of acetate. However, due to the reaction of CO_2 and KOH forming carbonate, CO_2 is not a proper reaction gas in alkaline reactors.

Given the inertness of CO in alkaline electrolytes, the CO reduction reaction (CORR) instead of CO_2RR can be conducted in alkaline reactors, which could increase the charge transfer rates, suppress the competition of hydrogen evolution reaction (HER) and improve the acetate FE [19,20]. Moreover, *CO is known as a vital intermediate for the formation of multi-carbon (C_{2+}) products in CO_2RR [21–23], and thus CORR is potentially more direct for C_2 electroproduction.

To date, copper is the state-of-the-art catalyst for the electro-conversion of CO_2/CO to C_2 products. Lots of strategies, including morphological modification [24,25], grain boundary control [26], reaction condition optimization [19], introducing various elements as modulators [14] and modifying the local oxidation state of Cu [10,27], have been taken to enhance the selectivity of C_2 products and the current density. Surface Cu^+ active sites modulated by non-metal elements have been proved theoretically and experimentally to greatly improve the selectivity of C_2 products [10,12,28]. However, the oxygen-modulated Cu^+ species, always derived from cuprous oxide (Cu_2O) and copper oxide (CuO), is extremely unstable and tends to be reduced to Cu^0 species under CO_2/CORR conditions, leading to decreased catalytic performance [29].

In contrast to the instability of oxygen-modulated Cu^+, copper nitride has been reported to be stable during CO_2 reduction [30,31]. Negligible degradation of high C_{2+} product FEs was achieved on a Cu-on-Cu_3N catalyst in 30 h, suggesting that nitrogen (N) could be a competent stabilizer to maintain the Cu^+ state [30]. In addition, doping N also provides a more favorable pathway for the reduction of CO_2 to acetate, and a remarkable FE of acetate ($FE_{acetate}$) (nearly 78%) was achieved on a N-doped nanodiamond/Si rod array [32], but the acetate partial current density was lower than 1 mA cm^{-2}. Inspired by the above studies, we therefore explore whether incorporating N into Cu catalysts could preserve Cu^+ species and further improve the current density and $FE_{acetate}$ in CORR.

We firstly sought to use density function theory (DFT) to testify the existence of Cu^+ species modulated by incorporating N into Cu and then investigated its effect on the selectivity of products in CORR. Bader charge analysis, as shown in Fig. 1b, presents the obvious difference

[1] State Key Laboratory of Molecular Engineering of Polymers, Department of Macromolecular Science and Laboratory of Advanced Materials, Fudan University, Shanghai 200438, China
[2] Institute of Functional Nano & Soft Materials (FUNSOM) and Jiangsu Key Laboratory for Carbon-Based Functional Materials & Devices, Soochow University, Suzhou 215123, China
* Corresponding authors (emails: tcheng@suda.edu.cn (Cheng T); bozhang@fudan.edu.cn (Zhang B); penghs@fudan.edu.cn (Peng H))

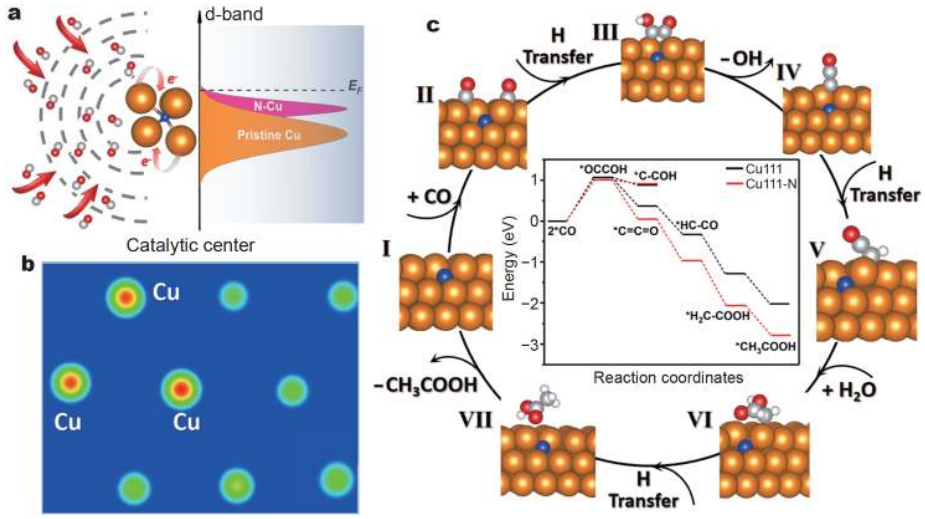

Figure 1 Schematic illustration of acetate electrosynthesis process. (a) Schematic illustration for the synthesis process of acetate using N-Cu catalyst, and the comparison of DOS between pristine Cu and N-Cu systems, where E_F refers to Fermi level. Color code: Cu (brown), N (blue), C (light gray), O (red). (b) Bader charge analysis of the first layer Cu atoms from the constructed N-Cu model. (c) Free energy profiles of acetate formation on Cu (111) and N-Cu (111) surface, respectively. The optimized structures of key intermediates during CORR on N-Cu (111) are shown in the reaction cycle.

of charge density with respect to the first layer Cu atoms in N-modulated Cu (denoted as N-Cu), indicating that the presence of N withdraws electrons from nearby Cu atoms, further resulting in three positively charged Cu^+ with formal charge from 0.25 to 0.35 e (Fig. S1). The existence of N also shifts the electronic density of state (DOS) toward Fermi energy (Fig. 1a), referring to a decrease of work function, which is consistent with the charge analysis.

Indeed, from our DFT calculations, we predicted that the presence of N decreases the formation energy of *OC–COH, as the potential determining step (PDS) of C_2 products, by ~0.1 eV, as shown in Fig. 1c. The selectivity among different C_2 products, such as ethylene, ethanol and acetate, is determined by the branching of reaction pathways after *OC–COH. Cheng and coworkers [33] found that the branching of ethylene and acetate is in the early stage after forming *OC–COH, and distinguished *C=C=O as a key intermediate toward acetate formation. The formation of *C=C=O is likely from the dehydration of *HOC–COH *via* a non-electrochemical reaction. Meanwhile, *HOC–COH can be electrochemically converted to *C–COH, which is the precursor of ethylene and ethanol formation [34]. Thus, we considered the reactions from *HOC–COH to *C–COH or *C=C=O in our DFT simulation to predict the selectivity of acetate on N-Cu.

As demonstrated in Fig. 1c, compared with pure Cu, N dopant significantly lowers the formation energy of *C=C=O by 0.36 eV, while the formation of *C–COH is slightly destabilized by 0.066 eV. Both these trends work in the same direction of promoting the selectivity towards acetate formation. We also calculated the following reactions to complete the reaction pathway of acetate formation. All the remaining reaction steps are exothermic. Thus, according to DFT calculations, we predicted that introducing N to Cu metal to form Cu^+ could be a feasible strategy to enhance acetate production.

Inspired by the DFT prediction, we sought to incorporate N atoms into Cu lattice *via* a solvothermal synthesis. The as-prepared catalyst was firstly characterized by transmission electron microscopy (TEM) (Fig. 2a). The catalyst demonstrated an irregular morphology, with a particle size of 100–200 nm. The elemental mapping obtained by energy-dispersive X-ray spectroscopy (EDX) (Fig. S2) indicated that N was homogeneously distributed in the Cu. High-resolution TEM (HRTEM) results showed that the inter-planar spacing of N-Cu is 2.166 Å, slightly larger than that (2.113 Å) of commercial Cu (Com-Cu). As the N anion possesses a larger ionic radius than Cu ion, the insertion of N may cause the lattice expansion [35]. These structural distortions were further validated by the powder X-ray diffraction (XRD). As shown in Fig. 2d, the (111), (200) and (220) planes of cubic copper correspond to the diffraction peaks at around 43.3°, 50.4° and 74.1°, respectively. While the diffraction patterns of Com-Cu and N-Cu are very similar, the diffraction peak of N-Cu

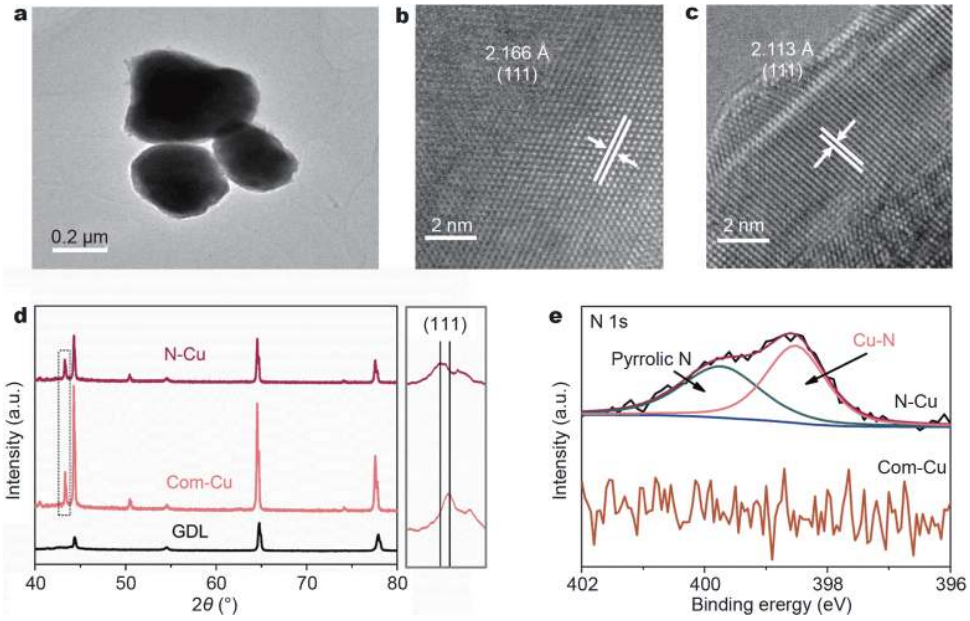

Figure 2 The structural characterizations of N-Cu and Com-Cu. (a) TEM image of N-Cu. (b, c) The HRTEM images of N-Cu (b) and Com-Cu (c). (d) XRD patterns of Com-Cu and N-Cu and the partial magnification of the corresponding diffraction peaks of the (111) facet. (e) XPS N 1s spectra of Com-Cu and N-Cu.

corresponding to (111) facet has slightly shifted to the lower angle region with the incorporation of N. This slight deviation suggests that N doping does not alter the intrinsic structure of metallic Cu but results in a mildly enlarged inter-planar distance. These results point out that N has been successfully introduced into the Cu lattice.

We further conducted X-ray spectroscopy to investigate the chemical states of surface Cu and N atoms. The X-ray photoelectron spectroscopy (XPS) spectrum of N 1s (Fig. 2e) in N-Cu exhibited that the peak located at 398.5 eV is indexed to the Cu–N bond [31]. Meanwhile, soft X-ray absorption spectroscopy (sXAS) was also conducted to examine the existence of N. From the N *K*-edge sXAS profile of the sample (Fig. S3), the obvious peak in N-Cu verified the presence of N.

To further explore the chemical state of Cu after CORR, we conducted the *ex-situ* XPS and Cu L_3-edge sXAS spectra of N-Cu and Com-Cu as control samples. In the typical Cu 2p XPS spectra, two peaks at 933 and 952.8 eV are ascribed to the Cu $2P_{3/2}$ and Cu $2P_{1/2}$ of Cu^0, while the relative two Cu^{2+} peaks of Com-Cu are at 934.5 and 955 eV. But the two peaks of N-Cu are obviously broader (Fig. 3a), confirming that its surfaces are enriched with Cu^+ sites [30]. The residual N in N-Cu also verifies the stable structure of N-modulated Cu^+ during the CO reduction (Fig. 3b). As depicted in Fig. 3c, the larger peak located at 934.8 eV of N-Cu ascertains the presence of surface Cu^+ [36–38]. The above results prove the existence of surface Cu^+ modulated by N dopant, which is consistent with the DFT simulation results, indicating a promise for improving the production of acetate.

To further verify the effect of N-modulated Cu^+ active sites on CORR performance, we conducted chronopotentiometry experiments on N-Cu (Figs S4–S6), and chose Com-Cu (Figs S7–S10) and Cu_2O nanoparticles as control samples (Figs S11–S14). All tests were carried out in a three-electrode flow cell system in 2.0 mol L^{-1} KOH aqueous electrolyte to eliminate the mass transport limitation [39]. A maximal $FE_{acetate}$ of 42% was obtained on N-Cu at the potential of −1.27 V *vs.* reversible hydrogen electrode (RHE), while the Com-Cu exhibited an $FE_{acetate}$ of 29% (Fig. 4a, b). Furthermore, the highest $FE_{acetate}$ of Cu_2O (Fig. S13) was 12%, suggesting that Cu_2O had significantly poorer selectivity of CORR to acetate than N-Cu. However, the FEs of other C_{2+} products of Com-Cu and Cu_2O at lower potentials were all higher than the equivalents of N-Cu. As reflected, this N-modulated Cu^+ strategy dramatically improves the selectivity of acetate by suppressing the formation of ethylene and ethanol, in comparison with Com-Cu and Cu_2O.

To further investigate the CORR performance, we conducted the cyclic voltammograms on the catalysts in 2 mol L^{-1} KOH aqueous electrolyte at the scan rate of

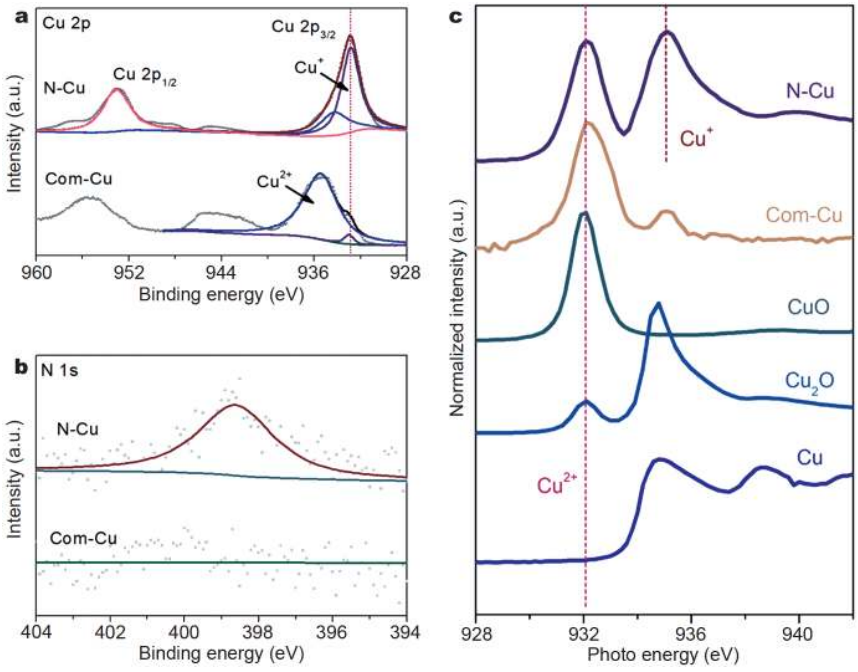

Figure 3 Characterizations of the surface chemical state of Cu in catalysts after reaction. (a, b) XPS Cu 2p and N 1s spectra of Com-Cu and N-Cu after 30-min reduction of CO, respectively. (c) Soft XAS of Cu L_3-edge for Com-Cu and N-Cu after CORR for 30 min.

50 mV s^{-1}. The linear sweep voltammetry curves in Fig. 4c reveal that the cathodic currents of the two samples quickly increase as the applied potential is more negative than −0.5 V *vs.* RHE. In addition, compared with Com-Cu, a larger increase of current density for N-Cu was acquired, indicating that N-Cu exhibited higher CO reduction activity. As illustrated in Fig. 4d, the acetate partial current densities of N-Cu and Com-Cu both increase considerably, demonstrating remarkable transfer of CO to the triple-phase reaction interface. Moreover, the highest acetate partial current density of 180 mA cm^{-2} was achieved at −1.37 V on N-Cu, which is superior to the performance on Com-Cu, Cu_2O (Fig. S12) and the state-of-the-art catalysts [19,20,39–41] (Fig. 4e, Table S1), indicating that surface N-modulated Cu^+ active sites remarkably boosted the catalytic activity of Cu. Furthermore, the acetate turnover frequency (TOF) [42] exhibited the same tendency for the N-Cu. The TOF of N-Cu is ~0.048 s^{-1} per total Cu atoms at −1.37 V, approximately twice higher than that for Com-Cu. In sum, the highest $FE_{acetate,}$ highest acetate partial current densities and the TOF indicate that the Cu^+ species on N-Cu present a higher reduction rate and higher catalytic activity towards acetate.

To further understand the experimental mechanistic pathways for the CORR in the N-Cu catalyst, the Tafel slope derived from three partial current densities was investigated. Fig. 4f shows the slope values of N-Cu and Com-Cu, which are 176 and 197 mV per decade, respectively. For both samples, their slope values are close to 118 mV per decade, indicating that the rate-determining step of the CORR is the dimerization of two surface-adsorbed *CO [41,43]. In comparison with Com-Cu, N-Cu owned a lower Tafel slope, revealing superior CO reduction catalytic kinetics on N-Cu. Additionally, to further examine the stability of N-Cu, we tested its performance at a constant current density of 250 mA cm^{-2} in 2 mol L^{-1} KOH electrolyte (Fig. S15). The applied potential changed little over the course of 1 h of electrolysis with gradual increase and sudden decrease, which arose from the gradual formation and sudden disappearance of gas bubbles in the liquid catholyte chamber.

In summary, with the help of DFT prediction, we proposed a N modification strategy to modulate the electronic structure of Cu-based electrocatalysts. The N-modulated Cu^+ catalyst was highly active and can switch the intermediate transfer from *COCOH towards *CCO —the vital intermediate dominating the acetate formation. XPS, XAS and electrochemical studies well elaborated the link between highly efficient conversion of CO to acetate and the positively charged copper. Our N-doped Cu catalyst achieved an $FE_{acetate}$ of 42% with a

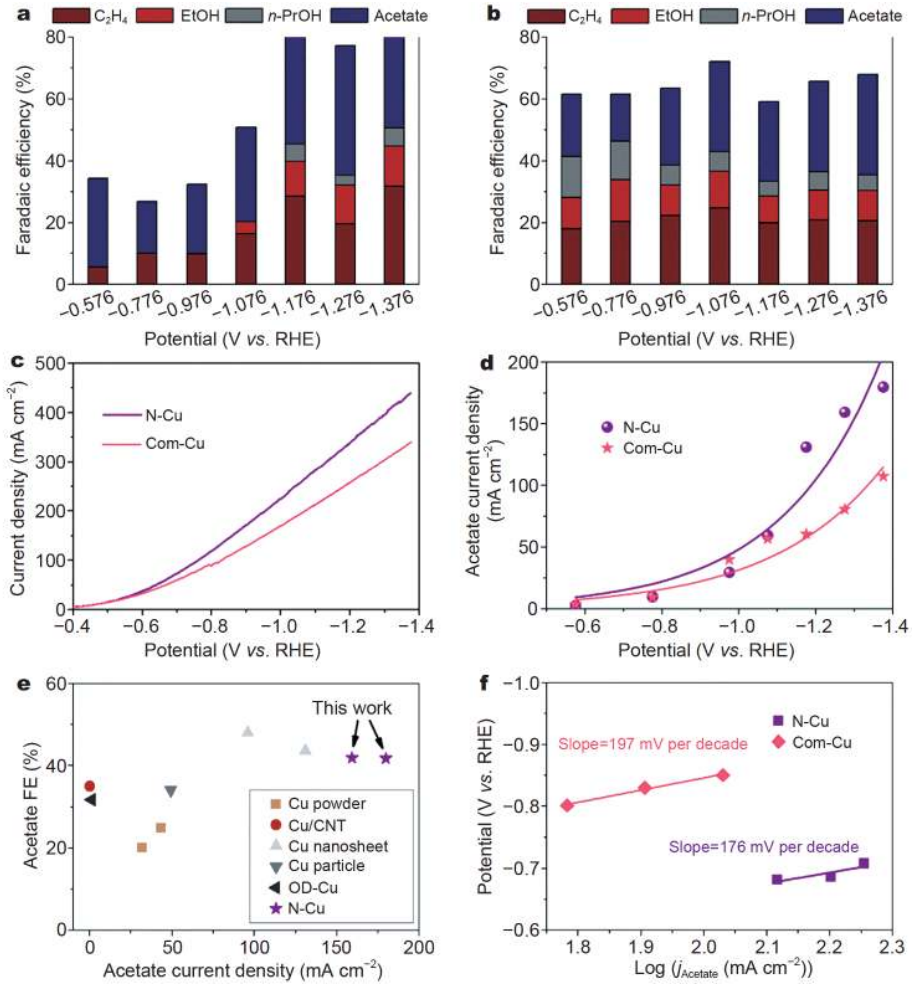

Figure 4 CO reduction performances of N-Cu and Com-Cu in a flow cell system. (a, b) FEs of CORR products on N-Cu (a) and Com-Cu (b) at various applied potentials in 2 mol L^{-1} KOH electrolyte. (c, d) The electrochemical reduction of CO polarization curves (c) and acetate partial current densities *versus* applied potentials (d) of Com-Cu and N-Cu. (e) The comparison of FEs and partial current densities for acetate between this work and state-of-the-art CO reduction systems [19,20,39–41]. (f) Tafel slopes derived from partial current densities for Com-Cu and N-Cu.

superior partial current density of 180 mA cm^{-2}. These findings may improve the electrocatalyst design in the future and promote the industrial application of CO_2RR/CORR technologies.

Received 20 May 2020; accepted 25 June 2020; published online 7 September 2020

1 Jhong HR, Ma S, Kenis PJ. Electrochemical conversion of CO_2 to useful chemicals: current status, remaining challenges, and future opportunities. Curr Opin Chem Eng, 2013, 2: 191–199
2 Jouny M, Luc W, Jiao F. General techno-economic analysis of CO_2 electrolysis systems. Ind Eng Chem Res, 2018, 57: 2165–2177
3 Seh ZW, Kibsgaard J, Dickens CF, *et al.* Combining theory and experiment in electrocatalysis: insights into materials design. Science, 2017, 355: eaad4998
4 Ma M, Trześniewski BJ, Xie J, *et al.* Selective and efficient reduction of carbon dioxide to carbon monoxide on oxide-derived nanostructured silver electrocatalysts. Angew Chem Int Ed, 2016, 55: 9748–9752
5 Liu M, Pang Y, Zhang B, *et al.* Enhanced electrocatalytic CO_2 reduction *via* field-induced reagent concentration. Nature, 2016, 537: 382–386
6 Won DH, Shin H, Koh J, *et al.* Highly efficient, selective, and stable CO_2 electroreduction on a hexagonal Zn catalyst. Angew Chem Int Ed, 2016, 55: 9297–9300
7 He S, Ni F, Ji Y, *et al.* The p-orbital delocalization of main-group metals to boost CO_2 electroreduction. Angew Chem Int Ed, 2018, 57: 16114–16119
8 Gao S, Jiao X, Sun Z, *et al.* Ultrathin Co_3O_4 layers realizing optimized CO_2 electroreduction to formate. Angew Chem Int Ed, 2016, 55: 698–702
9 Klinkova A, De Luna P, Dinh CT, *et al.* Rational design of efficient palladium catalysts for electroreduction of carbon dioxide to formate. ACS Catal, 2016, 6: 8115–8120

10 Mistry H, Varela AS, Bonifacio CS, *et al.* Highly selective plasma-activated copper catalysts for carbon dioxide reduction to ethylene. Nat Commun, 2016, 7: 12123
11 Dinh CT, Burdyny T, Kibria MG, *et al.* CO_2 electroreduction to ethylene *via* hydroxide-mediated copper catalysis at an abrupt interface. Science, 2018, 360: 783–787
12 Bai H, Cheng T, Li S, *et al.* Controllable CO adsorption determines ethylene and methane productions from CO_2 electroreduction. Sci Bull, 2020, doi: 10.1016/j.scib.2020.06.023
13 Li YC, Wang Z, Yuan T, *et al.* Binding site diversity promotes CO_2 electroreduction to ethanol. J Am Chem Soc, 2019, 141: 8584–8591
14 Hoang TTH, Verma S, Ma S, *et al.* Nanoporous copper–silver alloys by additive-controlled electrodeposition for the selective electroreduction of CO_2 to ethylene and ethanol. J Am Chem Soc, 2018, 140: 5791–5797
15 Ma S, Sadakiyo M, Heima M, *et al.* Electroreduction of carbon dioxide to hydrocarbons using bimetallic Cu–Pd catalysts with different mixing patterns. J Am Chem Soc, 2017, 139: 47–50
16 Munir S, Varzeghani AR, Kaya S. Electrocatalytic reduction of CO_2 to produce higher alcohols. Sustain Energy Fuels, 2018, 2: 2532–2541
17 Wang Y, Wang D, Dares CJ, *et al.* CO_2 reduction to acetate in mixtures of ultrasmall $(Cu)_m(Ag)_m$ bimetallic nanoparticles. Proc Natl Acad Sci USA, 2018, 115: 278–283
18 Li CW, Ciston J, Kanan MW. Electroreduction of carbon monoxide to liquid fuel on oxide-derived nanocrystalline copper. Nature, 2014, 508: 504–507
19 Jouny M, Luc W, Jiao F. High-rate electroreduction of carbon monoxide to multi-carbon products. Nat Catal, 2018, 1: 748–755
20 Luc W, Fu X, Shi J, *et al.* Two-dimensional copper nanosheets for electrochemical reduction of carbon monoxide to acetate. Nat Catal, 2019, 2: 423–430
21 Liu X, Xiao J, Peng H, *et al.* Understanding trends in electrochemical carbon dioxide reduction rates. Nat Commun, 2017, 8: 15438
22 Kortlever R, Shen J, Schouten KJP, *et al.* Catalysts and reaction pathways for the electrochemical reduction of carbon dioxide. J Phys Chem Lett, 2015, 6: 4073–4082
23 Ou L, Long W, Chen Y, *et al.* New reduction mechanism of CO dimer by hydrogenation to C_2H_4 on a Cu(100) surface: theoretical insight into the kinetics of the elementary steps. RSC Adv, 2015, 5: 96281–96289
24 Zhuang TT, Liang ZQ, Seifitokaldani A, *et al.* Steering post-C–C coupling selectivity enables high efficiency electroreduction of carbon dioxide to multi-carbon alcohols. Nat Catal, 2018, 1: 421–428
25 Zhuang TT, Pang Y, Liang ZQ, *et al.* Copper nanocavities confine intermediates for efficient electrosynthesis of C_3 alcohol fuels from carbon monoxide. Nat Catal, 2018, 1: 946–951
26 Kim D, Kley CS, Li Y, *et al.* Copper nanoparticle ensembles for selective electroreduction of CO_2 to C_2–C_3 products. Proc Natl Acad Sci USA, 2017, 114: 10560–10565
27 Zhou Y, Che F, Liu M, *et al.* Dopant-induced electron localization drives CO_2 reduction to C_2 hydrocarbons. Nat Chem, 2018, 10: 974–980
28 Xiao H, Goddard Iii WA, Cheng T, *et al.* Cu metal embedded in oxidized matrix catalyst to promote CO_2 activation and CO dimerization for electrochemical reduction of CO_2. Proc Natl Acad Sci USA, 2017, 114: 201702405
29 Lee S, Kim D, Lee J. Electrocatalytic production of C_3–C_4 compounds by conversion of CO_2 on a chloride-induced bi-phasic Cu_2O-Cu catalyst. Angew Chem Int Ed, 2015, 54: 14701–14705
30 Liang ZQ, Zhuang TT, Seifitokaldani A, *et al.* Copper-on-nitride enhances the stable electrosynthesis of multi-carbon products from CO_2. Nat Commun, 2018, 9: 3828
31 Yin Z, Yu C, Zhao Z, *et al.* Cu_3N Nanocubes for selective electrochemical reduction of CO_2 to ethylene. Nano Lett, 2019, 19: 8658–8663
32 Liu Y, Chen S, Quan X, *et al.* Efficient electrochemical reduction of carbon dioxide to acetate on nitrogen-doped nanodiamond. J Am Chem Soc, 2015, 137: 11631–11636
33 Cheng T, Fortunelli A, Goddard Iii WA. Reaction intermediates during *operando* electrocatalysis identified from full solvent quantum mechanics molecular dynamics. Proc Natl Acad Sci USA, 2019, 116: 7718–7722
34 Lum Y, Cheng T, Goddard Iii WA, *et al.* Electrochemical CO reduction builds solvent water into oxygenate products. J Am Chem Soc, 2018, 140: 9337–9340
35 Cai J, Song Y, Zang Y, *et al.* N-induced lattice contraction generally boosts the hydrogen evolution catalysis of P-rich metal phosphides. Sci Adv, 2020, 6: eaaw8113
36 Sham TK, Hiraya A, Watanabe M. Electronic structure of Cu-Au alloys from the Cu perspective: A $CuL_{3,2}$-edge study. Phys Rev B, 1997, 55: 7585–7592
37 Li J, Che F, Pang Y, *et al.* Copper adparticle enabled selective electrosynthesis of n-propanol. Nat Commun, 2018, 9: 4614
38 Hulbert SL, Bunker BA, Brown FC, *et al.* Copper $L_{2,3}$ near-edge structure in Cu_2O. Phys Rev B, 1984, 30: 2120–2126
39 Ripatti DS, Veltman TR, Kanan MW. Carbon monoxide gas diffusion electrolysis that produces concentrated C_2 products with high single-pass conversion. Joule, 2019, 3: 240–256
40 Feng X, Jiang K, Fan S, *et al.* A direct grain-boundary-activity correlation for CO electroreduction on Cu nanoparticles. ACS Cent Sci, 2016, 2: 169–174
41 Li J, Chang K, Zhang H, *et al.* Effectively increased efficiency for electroreduction of carbon monoxide using supported polycrystalline copper powder electrocatalysts. ACS Catal, 2019, 9: 4709–4718
42 Zhang L, Yuan H, Wang L, *et al.* The critical role of electrochemically activated adsorbates in neutral OER. Sci China Mater, 2020, 63: 2509–2516
43 Xiao H, Cheng T, Goddard Iii WA, *et al.* Mechanistic explanation of the pH dependence and onset potentials for hydrocarbon products from electrochemical reduction of CO on Cu (111). J Am Chem Soc, 2016, 138: 483–486

Acknowledgements This work was supported by the Ministry of Science and Technology (2016YFA0203302), the National Natural Science Foundation of China (21875042, 21634003, 51573027 and 21975148), the Science and Technology Commission of Shanghai Municipality (16JC1400702 and 18QA1400800), Shanghai Municipal Education Commission (2017-01-07-00-07-E00062), the Program of Eastern Scholar at Shanghai Institutions and Yanchang Petroleum Group, the Natural Science Foundation of Jiangsu Higher Education Institutions (SBK20190810), Jiangsu Province High-Level Talents (JNHB-106), the China Postdoctoral Science Foundation (2019M660128), the start-up supports of Soochow University and the Program for Jiangsu Specially-Appointed Professors, and the Priority Academic Program Development of Jiangsu Higher Education Institutions (PAPD). We acknowledge Shanghai Supercomputer Center for providing the computational re-

sources, and Collaborative Innovation Center of Suzhou Nano Science & Technology for this work. This work also benefited from the 4B9B beamlines at Beijing Synchrotron Radiation Facility (BSRF).

Author contributions Peng H, Zhang B and Cheng T supervised the project. Yang H and Cheng T performed the DFT simulations. Ni F and Wen Y carried out the synthesis of catalysts and electrochemical measurements. Bai H and Zhang L performed the TEM experiments. Cui C, Li S and He S performed the sXAS experiments. All authors discussed the results and helped with the the manuscript preparation.

Conflict of interest The authors declare that they have no conflict of interest.

Supplementary information Experimental details and supporting data are available in the online version of the paper.

Fenglou Ni received his BE in functional materials from Huazhong University of Science and Technology in 2017. He is a Master candidate in the Laboratory of Advanced Materials at Fudan University. His research is focused on electrochemistry, energy conversion and storage.

Bo Zhang received his BE in applied physics from Northwestern Polytechnical University in 2006, and his PhD in chemical engineering and technology from East China University of Science and Technology in 2011. He then worked at East China University of Science and Technology from 2011 to 2015, and the University of Toronto from 2015 to 2017. He is currently a full professor in the Department of Macromolecular Science at Fudan University. His research is focused on electrochemistry, energy conversion and storage.

氮调控正价态铜用于高效电化学还原一氧化碳制备乙酸

倪凤楼[1], 杨昊[2], 温蕴周[1], 白海鹏[1], 张龙生[1], 崔春雨[1], 李尚育[1], 何思斯[1], 程涛[2*], 张波[1*], 彭慧胜[1*]

摘要 利用间歇性可再生能源电转化二氧化碳和一氧化碳制备多碳工业原料和燃料能够完善碳循环. 然而, 二氧化碳转化为乙酸的法拉第效率难以满足大规模应用的要求. 研究发现, 调控铜的局域电子结构至正价态, 以及使用一氧化碳作为反应气均能够提高多碳产物的选择性. 因此, 我们提出杂原子调控策略, 用于调节催化剂表面活性位点的氧化态. 密度泛函理论研究表明, 掺杂氮原子调控正价态铜位点, 在热力学上有利于形成中间体*CCO, 进而生成乙酸. 我们进一步利用溶剂热法合成氮掺杂的铜催化剂, 并通过软X射线吸收谱和X射线光电子能谱证实催化剂表面存在大量正价态铜位点. 同时, 该催化剂在一氧化碳还原反应中实现了42%的乙酸法拉第效率和已知最高的乙酸偏电流密度180 mA cm^{-2}.

